Acta Materialia 139 (2017) 174–187

Contents lists available at ScienceDirect

Acta Materialia

journal homepage: www.elsevier.com/locate/actamat

Full length article

Interfacial stresses within boundary between martensitic variants: Analytical and numerical finite strain solutions for three phase field models

Anup Basak [a], Valery I. Levitas [a, b, c, *]

[a] Department of Aerospace Engineering, Iowa State University, Ames, IA 50011, USA
[b] Departments of Mechanical Engineering and Material Science and Engineering, Iowa State University, Ames, IA 50011, USA
[c] Ames Laboratory, Division of Materials Science and Engineering, Ames, IA 50011, USA

ARTICLE INFO

Article history:
Received 13 May 2017
Received in revised form
5 July 2017
Accepted 30 July 2017
Available online 2 August 2017

Keywords:
Phase field method
Martensitic phase transformation
Variant-variant boundary
Strain incompatibility
Interfacial stresses

ABSTRACT

The origin of a large elastic stress within an interface between martensitic variants (twins) within a finite strain phase field approach has been determined. Notably, for a sharp interface this stress is absent. Three different constitutive relations for the transformation stretch tensor versus order parameters have been considered: a linear combination of the Bain tensors (kinematic model-I, KM-I), an exponential-logarithmic combination (KM-II) of the Bain tensors, and a stretch tensor corresponding to simple shear (KM-III). An analytical finite-strain solution has been found for an infinite sample for tetragonal martensite under plane stress condition. In particular, explicit expression for the stresses have been obtained. The maximum interfacial stress for KM-II is more than twice that which corresponds to KM-I. Stresses are absent for KM-III, but it is unclear how to generalize this model for multivariant martensitic transformation. An approximate analytical solution for a finite sample has been found as well. It shows good correspondence with numerical results obtained using the finite element method. The obtain results are important for developing phase field approaches for multivariant martensitic transformations coupled to mechanics, especially at the nanoscale.

1. Introduction

Interfacial stresses. Interfacial stresses play an important role in the formation of the nanostructures, causing martensitic phase transformations (PTs) in the nanowires [1,2], and influencing the nucleation condition and evolution in the multivariant martensitic microstructures [3,4]. Interfacial stresses can also reduce the activation energy for intermediate melt nucleation within solid-solid interface by more than an order of magnitude [5]. Interfaces may have a complex internal structure, including the intermediate phases [6–9]. They may appear as an intermediate state during PTs, e.g., solid-solid PT via intermediate melting [10–15]. Interfacial stresses have been determined for external surfaces [1] and solid-melt interfaces [16–18] using atomistic simulations.

It is well-known [19] that each material surface is subjected to biaxial interface stresses. For phases that do not support deviatoric stresses at the equilibrium (liquids and gases), the interfacial force per unit length $\overline{\sigma}^S$ in both directions is equal to the surface energy γ. For interfaces in solids, or for solid-liquid and solid-gas interfaces, the magnitude of the surface stresses is determined by the Shuttleworth equation [20] $\overline{\sigma}^S = \gamma + \partial\gamma/\partial\varepsilon_i = \overline{\sigma}_{st} + \overline{\sigma}_e^S$, where ε_i is the mean interface strain. Thus, interfacial stress consists of two parts: the tensile structural stress, $\overline{\sigma}_{st}$, which is the same as for a liquid-gas interface, and another, $\overline{\sigma}_e^S$, which is caused by elastic deformation of an interface and which may be tensile or compressive.

Within the sharp interface approach, the constitutive equations and balance laws for elastic interfaces were derived in Refs. [20–27]. The challenges are (a) in finding the material parameters and (b) in the concern for whether the resultant interfacial stresses can be formalized through simple constitutive equations due to strongly heterogeneous interfacial fields like elastic moduli, transformation strains, and total strains across the interface.

Phase field approach. The phase field approach, which for the

* Corresponding author. Department of Aerospace Engineering, Iowa State University, Ames, IA 50011, USA.
E-mail address: vlevitas@iastate.edu (V.I. Levitas).

http://dx.doi.org/10.1016/j.actamat.2017.07.059
1359-6454/

conserved order parameters is also known as the Ginzburg-Landau approach, is broadly applied for studying the microstructure evolution during various first-order PTs. The most relevant to the current paper are works on modeling austenite - multivariant martensite and twinned microstructure evolution in crystalline solids [4,28–41]. We also mention works on transformations in liquids [42] and melting/solidification [43–45], in which interfacial stresses have been included. In the phase field models, the interface has a finite width, and its structure (i.e., distribution of all fields within an interface) is resolved. Interfacial stresses σ_{st} (here, force per unit area at each point within the interface) with the resultant force per unit length $\overline{\sigma}_{st}$ equal to the interface energy γ have been introduced in Refs. [42–44], but are not fully consistent; see the discussion in Ref. [46]. The problem of introducing of the interfacial stresses σ_{st} was solved for melting [47,48] and the solid-solid interface for small [3,46,49] and large [50,51] strains, including cases with anisotropic interface energy [51]. The interfacial stresses were also introduced and studied for a complex solid-melt-solid interface [5,52], which appears during solid-solid PT via the intermediate melt.

Elastic interfacial stresses σ_e^S (with resultant force per unit interface length $\overline{\sigma}_e^S$) appear automatically (i.e., without extra terms in the constitutive equations) as a result of solution of the coupled Ginzburg-Landau and elasticity equations, due to heterogeneity of the transformations strain and the elastic properties within interface. They were found numerically for a solid-melt interface [45,47,48], for the austenite-martensite [3] and martensite-martensite [4,33] interfaces, as well as for a complex solid-melt-solid interface [5,52,53]. In contrast, the theory in Ref. [54] introduces the explicit dependence of the gradient energy on the interfacial strain. This results in the additional interfacial stresses that depend on the gradient of the order parameter. In the sharp interface limit, this theory reduces to the theory in Ref. [23], in which interfacial energy depends on the interfacial strain. The theory in Ref. [54] does not include structural interfacial stresses σ_{st}. Since the boundary-value problem for stresses was not solved in Ref. [54], elastic stresses due to heterogeneity of material parameters within the interface were not discussed. At the same time, it is argued in Ref. [50] that it is not evident that such an additional dependence of the gradient energy on the interfacial strain is necessary, because stresses due to heterogeneous distribution of material parameters across an interface (neglected in Ref. [54]) may be large, exceeding what one wants to introduce. This was shown for the solid-melt interface in Refs. [47,48]. In this case, volumetric transformation strain (more precisely, the biaxial part of the transformation strain along the interface) determines the elastic interfacial stresses [47,48]. They appeared to be too large and unrealistic (they are significantly larger than stresses determined using molecular dynamic simulations in Refs. [16,17]). These stresses artificially suppress melting, and in order to restore consistency with experimental data on the size-dependence of the melting temperature for Al nanoparticles, various methods of their relaxation (in particular, introducing an additional equation for stress relaxation) have been proposed in Refs. [47,48]. This led to the conclusion that for melting it is not necessary to introduce additional elastic interface stresses. However, there have been only limited attempts to understand which parameters affect elastic interfacial stresses for a solid-solid interface and how they can be controlled; see, e.g., [4,55,56].

In the current paper, we have found a complete analytical solution for the simplest case of a solid-solid interface between two martensitic variants, or a twin interface. Since transformation strain for twinning is a simple shear, internal stresses do not appear within the sharp interface between martensitic variants or twins. It is intuitively expected that they should not appear within a phase field approach also. However, we will see that this is not the case.

Multivariant martensitic PTs. Microstructure evolution during martensitic PTs plays the central role in determining mechanical, electrical, and other properties in a broad range of materials, e.g. shape memory alloys, ferroelectric materials, and multiferroic materials. The microstructures in such materials usually consist of mixture of austenite, A, and N martensitic variants, M_i, where $i = 1, 2, \ldots, N$; see, e.g., [57,58]. Some of the martensitic variants can form twin boundaries that are coherent interfaces. Across a twin boundary, one variant can be obtained by simple shear deformation of the other. In experiments, one rarely sees interfaces between A and a single martensitic variant, since the stress-free lattices of A and M_i in most of the materials are not geometrically compatible (in the sense of Hadamard's compatibility) to form a coherent stress-free interface. The system prefers to form microstructures consisting of A separated from twinned martensite by a plane interface, which minimizes the elastic energy of the system [57,58].

Various continuum theories [57–63] have been used to study twinned microstructures within sharp interface approaches. On the other hand, various aspects of the phase field approach to martensitic PTs and twinning have been developed and used for simulations in various papers; see e.g., [4,28–41]. The main concept is related to the order parameters η that describe material instabilities during PTs from A to M_i in a continuous way.

The necessary conditions for the Landau (local) potential and transformation strain, which are functions of the order parameters, have been formulated and utilized in Refs. [30,33,64–66] for small strains and in Refs. [30,67] for large strains. They, in particular, introduce the conditions that the thermodynamically equilibrium values of the order parameters are fixed (i.e., 0 or 1) for A and M_i for any stress and temperature and that the crystal lattice instability conditions should be included in the theory. This results in a much more complex expression for the thermodynamic potential and transformation strain tensor as compared to those used in the other theories [34–39]. Large strain formulation for multivariant martensitic PTs were developed in Refs. [30–32,38,39,67]. Three different kinematic assumptions are currently used in various papers.

(a) *Kinematic model-I (KM-I)*: Symmetric right transformational stretch $\boldsymbol{U}_t$ is considered as a linear combination of the Bain stretch tensors $\boldsymbol{U}_{ti}$ of all the martensitic variants multiplied with a corresponding nonlinear interpolation function of the order parameters [30,67]. Such an expression satisfies all of the conditions formulated in Refs. [30,67]. However, as it was shown in Refs. [38,39], it does not conserve the determinant of the transformation stretch (i.e., volumetric transformation strain) within the transition region between the variants where $0 < \eta < 1$. In particular, this means that while all martensitic variants have the same specific volume, the transformation process $M_i \leftrightarrow M_j$ is not isochoric. This requirement is not a mandatory one, because, for dislocational slip, for example, there is a volume change along the shearing process between two stable atomic configurations [68]. In fact, defect cores in dislocations and twin boundaries may induce change in volume (see Chapter 7 and 8 of [69] and the references therein). However, the requirement for volume conservation sounds reasonable, at least, for the simplest model; it is good to have such a model. If volume change is observed during a transformation process between two martensitic variants, in principle, it could be included as a correction to the isochoric model.

(b) *Kinematic model-II (KM-II)*: Recently, an alternative expression for the transformation stretch was proposed, which is given by exponential of a linear combination of the natural logarithm of the Bain tensors [38,39]. In this case, the volume remains always preserved along the entire path of the $M_i \leftrightarrow M_j$ transformations. However, numerical simulations demonstrated large elastic stresses within twin boundaries, which were suppressed by some computational tricks [38,39]. It is necessary to mention that the order parameters in Refs. [38,39] are the volume fractions of various phases and all interpolation functions are linear in order parameters, in contrast to [30,67]. The requirements formulated in Refs. [30,67] were not considered [38,39].

Note that even for small strains, while the difference between two of the above models would be expected to be vanishing, large elastic stresses within the $M_i - M_i$ interfaces have been reported in Refs. [4,33]. An unambiguous explanation for the reason of such large elastic stresses within twin boundaries is still missing. Needless to say, a proper understanding of the origin and nature of such stresses in twin boundaries is very important in order to use those models for further study and/or to develop a more suitable theory. Interfacial stresses can cause martensitic and variant-variant transformations [1,2]. Also, in a fine mixture of martensitic variants, their thickness is only a few nanometers and they possess sharp tips [70]. Large stresses within nanometer wide interfaces may cause significant stresses of the opposite sign in the bulk twin phases, which should strongly affect nucleation and evolution of a martensitic nanostructure [3,4].

(c) *Kinematic model-III (KM-III)*: When single twinning was studied, a simple shear assumption for the non-symmetric transformation deformation gradient $\boldsymbol{F}_t = \boldsymbol{I} + \gamma_t(\eta)\boldsymbol{m}\otimes\boldsymbol{n}$ was used [40,64,71]. Here, $\gamma_t(\eta) = \gamma_{t0}\phi(\eta)$ is a smooth function of the order parameter $0 \le \eta \le 1$ such that the interpolation function ϕ satisfies the conditions $\phi(0) = 0$, $\phi(1) = 1$, and $\partial\phi/\partial\eta(0) = \partial\phi/\partial\eta(1) = 0$ within the two variants, which were derived as the conditions for thermodynamic equilibrium of phases. Hence clearly, $\boldsymbol{F}_t = \boldsymbol{I}$ and $\boldsymbol{F}_t = \boldsymbol{I} + \gamma_{t0}\boldsymbol{m}\otimes\boldsymbol{n}$ within two respective variants, where γ_{t0} is the shear strain along the unit direction $\boldsymbol{m}$ in the plane with the unit normal $\boldsymbol{n}$ (called the twinning plane), and $\otimes$ stands for the dyadic product between two vectors. This model cannot be easily generalized for multiple martensitic variants; see Ref. [30]. To the best of our knowledge, the interfacial stresses for this model has not yet been studied.

Our goal is to investigate the origin of large elastic stresses within a variant M_1 - variant M_2 interface for all three phase field models, and to analyze the results in details. To accomplish this goal, an analytical finite strain solution has been obtained for all the fields within the plane $M_1 - M_2$ interface in an infinite sample under plane stress condition. Cubic A and tetragonal M_i have been considered. While for KM-III stresses within the interface were zero, significantly large stresses have been observed for KM-I and KM-II due to the heterogeneity in the components of the transformation deformation gradient tensor across the interface. In fact, for KM-II, the maximum value of the interfacial stress is more than twice of that for KM-I. Thus, if the goal is to develop a model with stress-free interfaces, one has to find a way of generalizing KM-III for multivariant transformations, and this is a challenging task. If one can tolerate interfacial stresses, but wants to minimize them, then the KM-I, which involves variation of the volumetric strain during $M_1 - M_2$ transformation, is better than the KM-II, which preserves volumetric strain. It also shows that the requirements to the phase field theories should be formulated not only for conditions when one phase homogeneously transforms into another one, but also for the case of coexistent phases divided by an interface. Furthermore, the effect of the finite size of a sample on the solutions has been investigated. An approximate analytical solution has been obtained for KM-I, and the finite element (FE) results for both KM-I and II have been presented. Analytical and numerical solutions for KM-I are in very good agreement.

The paper has been organized in the following manner. A system of coupled mechanics and phase field equations, and various constitutive relations have been listed in Section 2. We have presented our results for an infinite sample in Section 3 and for a finite sample in Section 4. We conclude our paper with Section 5.

We denote multiplication and inner product between two second order tensors as $(\boldsymbol{A}\cdot\boldsymbol{B})_{ij} = A_{ik}B_{kj}$ and $\boldsymbol{A} : \boldsymbol{B} = A_{ij}B_{ji}$, respectively, where repeated indices denote summation as per Einstein's convention; A_{ij} and B_{ij} are the components of the tensors in a right handed orthonormal Cartesian basis $\{\boldsymbol{e}_1, \boldsymbol{e}_2, \boldsymbol{e}_3\}$; determinant and trace of tensor $\boldsymbol{A}$ are denoted by $det\,\boldsymbol{A}$ and $tr\,\boldsymbol{A}$, respectively; subscript 0 means that the quantity is defined in the reference configuration Ω_0; superscripts T and -1 denote tensor transposition and inversion; the gradient operators in reference Ω_0 and deformed Ω configurations have been denoted by ∇_0 and ∇, respectively; $\boldsymbol{I}$ is the second order identity tensor; $\nabla_0^2 := \nabla_0\cdot\nabla_0$ denotes the Laplacian operator in Ω_0; $:=$ stands for equality by definition.

2. Coupled mechanics and phase field equations

We begin Section 2.1 by summarizing the standard kinematic relations, constitutive relations, and the Ginzburg-Landau equation for $M_1 \leftrightarrow M_2$ transformations. Stress-free A will be chosen as the reference configuration. A general theory for A and two martensitic variants requires at least two order parameters. Let us consider that one order parameter describes austenite $\leftrightarrow$ martensitic transformation such that it is 0 in A and 1 in M, and the other describes $M_1 \leftrightarrow M_2$ transformations (see Ref. [30] for a similar description). Hence if a system contains martensitic variants only and austenite is completely absent, then the order parameter related to austenite $\leftrightarrow$ martensitic transformation is equal to unity everywhere, and we just need a single order parameter for describing $M_1 \leftrightarrow M_2$ transformations. The system under study in the present paper primarily evolves with two variants, where the residual austenite is fully absent. We denote the later order parameter by η, where $\eta = 1$ in M_1 and $\eta = 0$ in M_2. Obviously, there would be only a single Ginzburg-Landau equation for the system under study. Next, specialized kinematic and constitutive relations based on plane stress assumption have been summarized in Section 2.2. Finally, the constitutive relations for the transformation stretch tensor $\boldsymbol{U}_t$ for cubic to tetragonal transformations have been collected in Section 2.3.

2.1. General theory and system of equations

2.1.1. Kinematics

The deformation of a transforming material is described by the smooth function $\boldsymbol{r} = \boldsymbol{r}(\boldsymbol{r}_0, t)$, where $\boldsymbol{r}$ and $\boldsymbol{r}_0$ are the position vectors of a particle in the deformed Ω and the reference Ω_0 configurations, respectively, and t denotes time. The deformation gradient $\boldsymbol{F} := \nabla_0\boldsymbol{r}$ is multiplicatively decomposed into elastic part $\boldsymbol{F}_e = \boldsymbol{V}_e\cdot\boldsymbol{R}$ and the symmetric transformation stretch tensor $\boldsymbol{U}_t$ (see Ref. [50] for details):

$$\boldsymbol{F}=\boldsymbol{F}_e\cdot\boldsymbol{U}_t=\boldsymbol{V}_e\cdot\boldsymbol{R}\cdot\boldsymbol{U}_t=\boldsymbol{V}_e\cdot\boldsymbol{F}_t;\quad \boldsymbol{F}_t=\boldsymbol{R}\cdot\boldsymbol{U}_t, \tag{2.1}$$

where $\boldsymbol{V}_e$ is the symmetric left elastic stretch tensor and $\boldsymbol{R}$ is the lattice rotation. The deformation gradient $\boldsymbol{F}$ maps an infinitesimal line element from Ω_0 to Ω; $\boldsymbol{U}_t$ is the mapping from Ω_0 to an intermediate stress-free configuration Ω_t; $\boldsymbol{F}_e$ maps Ω_t to the deformed configuration Ω. We define an Eulerian elastic strain tensor

$$\boldsymbol{b}_e=0.5(\boldsymbol{B}_e-\boldsymbol{I})=0.5\left(\boldsymbol{V}_e^2-\boldsymbol{I}\right), \tag{2.2}$$

where $\boldsymbol{B}_e:=\boldsymbol{F}_e\cdot\boldsymbol{F}_e^T$ is the left Cauchy-Green elastic strain tensor. The ratios of specific volumes in various configurations are defined as $J=det\ \boldsymbol{F}$, $J_t=det\ \boldsymbol{U}_t$, and $J_e=det\ \boldsymbol{F}_e$ with $J=J_eJ_t$. We define

$$\boldsymbol{\varepsilon}=\boldsymbol{V}-\boldsymbol{I},\quad \boldsymbol{\varepsilon}_t=\boldsymbol{U}_t-\boldsymbol{I},\quad \text{and}\quad \boldsymbol{\varepsilon}_e=\boldsymbol{V}_e-\boldsymbol{I}, \tag{2.3}$$

where $\boldsymbol{V}=\sqrt{\boldsymbol{F}\cdot\boldsymbol{F}^T}$ is the symmetric left total stretch tensor. The compatibility condition for the deformation gradient $\boldsymbol{F}$ is (see, e.g., Chapter 2 of [72])

$$\nabla_0\times\boldsymbol{F}=0,\quad \text{where}\quad (\nabla_0\times\boldsymbol{F})_{ij}=\varepsilon_{imn}\frac{\partial F_{jn}}{\partial r_{0m}} \tag{2.4}$$

denotes curl of $\boldsymbol{F}$ and ε_{imn} is the third order permutation tensor.

2.1.2. Constitutive relations and governing equations

We now collect the constitutive relations and the system of equations to be solved.

(i) *Mechanical equilibrium equation* for neglected body forces are:

$$\nabla_0\cdot\boldsymbol{P}=0\quad \text{in } \Omega_0, \tag{2.5}$$

where $\boldsymbol{P}$ is the nonsymmetric first Piola-Kirchhoff stress tensor.

(ii) *Helmholtz free energy density:* Neglecting the interfacial structural stresses σ_{st} we consider the Helmholtz free energy per unit mass as (see Ref. [50] for a more general form)

$$\psi(\boldsymbol{F}_e,\eta,\theta,\nabla_0\eta)=\frac{J_t}{\rho_0}\psi_e(\boldsymbol{F}_e,\eta,\theta)+A\eta^2(1-\eta)^2+0.5b|\nabla_0\eta|^2, \tag{2.6}$$

where ψ_e is the elastic free energy density per unit volume of Ω_t; the second term is the double-well barrier energy; and the third term is the gradient energy density, with A and b being corresponding parameters. For simplicity, isotropic St. Venant-Kirchhoff elastic material (see Chapter 5 of [72]) will be considered:

$$\overline{\psi}_e=0.5\lambda(tr\ \boldsymbol{b}_e)^2+\mu\boldsymbol{b}_e:\boldsymbol{b}_e, \tag{2.7}$$

where $\overline{\psi}_e(\boldsymbol{b}_e)=\psi_e(\boldsymbol{F}_e)$ and λ and μ are the Lamé constants, which are the same for both martensitic variants. Since elastic stresses in the problems below are quite small, linear stress-strain relation is justified. All derivations can be repeated for a linear anisotropic material; however, this will complicate equations without changing the main results significantly. Also, not all elastic constants for tetragonal martensite in NiAl alloy considered here are known; those which are known, are far from being precise, because they were found using molecular dynamics at zero temperature [73].

(iii) *Stress-strain relations:* Using the standard relations for the first Piola-Kirchhoff $\boldsymbol{P}$ and the Cauchy stress $\boldsymbol{\sigma}$ for isotropic materials, given by $\boldsymbol{P}=J\boldsymbol{\sigma}\cdot\boldsymbol{F}^{-T}$ and $\boldsymbol{\sigma}=J_e^{-1}\boldsymbol{V}_e^2\cdot(\partial\overline{\psi}_e/\partial\boldsymbol{b}_e)$ [50], we obtain

$$\begin{aligned}&\boldsymbol{\sigma}=J_e^{-1}\boldsymbol{V}_e^2\cdot(\lambda(tr\ \boldsymbol{b}_e)\boldsymbol{I}+2\mu\boldsymbol{b}_e),\quad \text{and}\\ &\boldsymbol{P}=J_t\boldsymbol{V}_e^2\cdot(\lambda(tr\ \boldsymbol{b}_e)\boldsymbol{I}+2\mu\boldsymbol{b}_e)\cdot\boldsymbol{F}^{-T}.\end{aligned} \tag{2.8}$$

(iv) *The stationary Ginzburg-Landau equation* for the order parameter η (see Ref. [50] for a detailed derivation)

$$\frac{\dot{\eta}}{L}=\left(\boldsymbol{P}^T\cdot\boldsymbol{F}_e-J_t\psi_e\boldsymbol{U}_t^{-1}\right):\frac{d\boldsymbol{U}_t}{d\eta}-2\rho_0A\eta\left(1-3\eta+2\eta^2\right)+b\frac{\partial^2\eta}{\partial r_{01}^2}=0, \tag{2.9}$$

where $L>0$ is the kinetic coefficient. We have assumed that η depends on the single coordinate r_{01}; see Section 3.

(v) *Boundary condition:* Assuming a phase-independent energy of the external surface S_0 of the body in Ω_0 we obtain

$$\nabla_0\eta\cdot\boldsymbol{n}_0=0\quad \text{on } S_0, \tag{2.10}$$

where $\boldsymbol{n}_0$ is the outward unit normal to S_0. All external surfaces are traction-free.

2.2. Plane stress condition: stresses and strains

For our goal, it is sufficient to consider the plane stress condition, i.e. $\sigma_{13}=\sigma_{23}=\sigma_{33}=0$. As a consequence, all out-of-plane components of $\boldsymbol{T}$ are also vanishing, and in $\boldsymbol{F}$, $\boldsymbol{F}_e$, $\boldsymbol{V}_e$, $\boldsymbol{R}$, and $\boldsymbol{U}_t$ all the off-diagonal out-of-plane (i.e. 13, 31, 23, and 32) components are identically zero. Using a standard procedure, the in-plane Cauchy stresses can be obtained as (see Chapter 7 of [74] for similar derivation with small strains)

$$\sigma_{ij}=J_e^{-1}V_{e\ ik}^2T'_{kj},\quad \text{where}\quad T'_{kj}=\lambda'(b_{ell})\delta_{kj}+2\mu b_{e\ kj}, \tag{2.11}$$

$\lambda'=2\mu\lambda/(\lambda+2\mu)$, δ_{kj} denotes the Kronecker delta, and the indices $i,j,k,l=1,2$. Also, it can be shown that $b_{e33}=-b_{eii}\lambda/(\lambda+2\mu)$. The relation $b_{e33}=0.5(F_{e33}^2-1)=0.5(V_{e33}^2-1)$ thus yields

$$F_{e33}=V_{e33}=\sqrt{1-\lambda' b_{eii}/\mu},\quad \text{and}\quad F_{33}=V_{e33}U_{t33}. \tag{2.12}$$

2.3. Constitutive relation for $\boldsymbol{U}_t$

Recall that our austenite and martensitic phases have cubic and tetragonal lattices, respectively. The Bain tensors for three variants are diagonal matrices of the form diag(β, α, α), diag(α, β, α), and diag(α, α, β), where α and β are constant parameters (see Chapter 4 of [58]). Here we consider the transformation between only two variants of martensite. Without loss of generality we will choose the first two Bain tensors. For convenience of analysis, we assume that the Bain tensors are rotated about $\boldsymbol{e}_3$ by $\pi/4$ (simply to get a twin boundary perpendicular to $\boldsymbol{e}_1$-axis, see Fig. 1(a)):

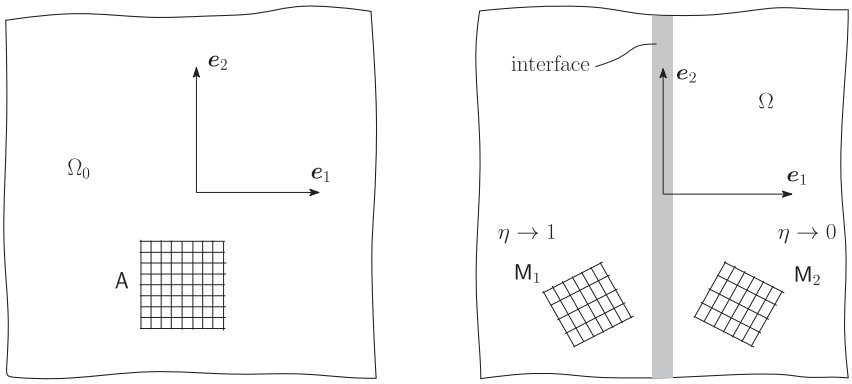

Fig. 1. Schematic diagram of an infinite body with lattice orientations: (a) stress-free reference configuration in the austenite phase; (b) deformed configuration with the twinned martensite; $\eta \to 1$ in M_1, $\eta \to 0$ in M_2; the interface has been indicated by the shaded region.

$$[\boldsymbol{U}_{t1}] = \begin{bmatrix} 0.5(\alpha+\beta) & 0.5(\alpha-\beta) & 0 \\ 0.5(\alpha-\beta) & 0.5(\alpha+\beta) & 0 \\ 0 & 0 & \alpha \end{bmatrix}, \quad [\boldsymbol{U}_{t2}] = \begin{bmatrix} 0.5(\alpha+\beta) & -0.5(\alpha-\beta) & 0 \\ -0.5(\alpha-\beta) & 0.5(\alpha+\beta) & 0 \\ 0 & 0 & \alpha \end{bmatrix}. \tag{2.13}$$

Three different constitutive relations for the transformation stretch tensor $\boldsymbol{U}_t$ will be discussed below.

KM-I: U_{ti} **based transformation rule.** In this model, $\boldsymbol{U}_t$ is expressed as a linear combination of $\boldsymbol{U}_{t1}$ and $\boldsymbol{U}_{t2}$ [30,33,67]:

$$\boldsymbol{U}_t = \boldsymbol{U}_{t2} + (\boldsymbol{U}_{t1} - \boldsymbol{U}_{t2})\phi(\eta), \tag{2.14}$$

in terms of the interpolation function

$$\phi = \eta^2(3-2\eta). \tag{2.15}$$

Other higher degree polynomials formulated in Refs. [64,65,67], satisfying the requirements $\phi(0)=0$, $\phi(1)=1$, and $\phi'(0)=\phi'(1)=0$, can also be used in the current paper without complications. Obviously, $\boldsymbol{U}_t = \boldsymbol{U}_{t1}$ and $\boldsymbol{U}_t = \boldsymbol{U}_{t2}$ for $\eta = 1$ (M_1) and $\eta = 0$ (M_2), respectively. Using Eq. (2.13) in Eq. (2.14) we get an explicit form:

$$[\boldsymbol{U}_t] = \begin{bmatrix} 0.5(\alpha+\beta) & 0.5(\beta-\alpha)(1-2\phi) & 0 \\ 0.5(\beta-\alpha)(1-2\phi) & 0.5(\alpha+\beta) & 0 \\ 0 & 0 & \alpha \end{bmatrix}. \tag{2.16}$$

The normal components of $\boldsymbol{U}_t$ given by Eq. (2.16) are constants, but the shear component U_{t12} is heterogeneous across the interface. Obviously, $det\ \boldsymbol{U}_t = 0.25\alpha[(\beta+\alpha)^2 - (\beta-\alpha)^2(1-2\phi)^2]$ is also heterogeneous across the interface, thereby indicating that the volume will not remain conserved during variant-variant transformation.

KM-II: $\ln U_{ti}$ **based transformation rule.** Alternatively, following [38,39], we assume $\boldsymbol{U}_t$ as exponential of linear combination of natural logarithm of the Bain tensors:

$$\boldsymbol{U}_t = \exp[\phi \ln U_{t1} + (1-\phi)\ln U_{t2}]. \tag{2.17}$$

The definitions of logarithm and exponential of tensors can be found, for example, in Chapter 1 of [72]. It is easy to verify from Eq. (2.17) that in pure M_1 and M_2, $\boldsymbol{U}_t = \boldsymbol{U}_{t1}$ and $\boldsymbol{U}_t = \boldsymbol{U}_{t2}$, respectively. Using the properties $det(\exp \boldsymbol{U}_{ti}) = \exp(tr\ \boldsymbol{U}_{ti})$ and $\ln(det\ \boldsymbol{U}_{ti}) = tr(\ln \boldsymbol{U}_{ti})$ (see Chapter 1 of [72]) one can show that

$$\begin{aligned} det\ \boldsymbol{U}_t &= det(\exp[\phi \ln U_{t1} + (1-\phi)\ln U_{t2}\,]) \\ &= \exp[\phi\ tr(\ln U_{t1}) + (1-\phi)\ tr(\ln U_{t2})\,] \\ &= \exp[\phi \ln(det\ U_{t1}) + (1-\phi)\ln(det U_{t2})\,] = det\ U_{ti}, \end{aligned} \tag{2.18}$$

where we have used the fact that $det\ \boldsymbol{U}_{t1} = det\ \boldsymbol{U}_{t2}$. Obviously, Eq. (2.18) proves that the transformation rule Eq. (2.17) conserves the volume during $M_1 \leftrightarrow M_2$ transformations. Using Eq. (2.13) in Eq. (2.17) and simplifying we write

$$[\boldsymbol{U}_t] = \begin{bmatrix} 0.5\left(\alpha^\phi\beta^{1-\phi} + \alpha^{1-\phi}\beta^\phi\right) & 0.5\left(\alpha^\phi\beta^{1-\phi} - \alpha^{1-\phi}\beta^\phi\right) & 0 \\ 0.5\left(\alpha^\phi\beta^{1-\phi} - \alpha^{1-\phi}\beta^\phi\right) & 0.5\left(\alpha^\phi\beta^{1-\phi} + \alpha^{1-\phi}\beta^\phi\right) & 0 \\ 0 & 0 & \alpha \end{bmatrix}. \tag{2.19}$$

From Eqs. (2.19) and Eq. (2.18) it is clear that $det\ \boldsymbol{U}_t = \alpha(U_{t11}U_{t22} - U_{t12}^2) = \alpha^2\beta$ is a constant.

KM-III: simple shear. In Refs. [40,64,71] and several other papers devoted to twinning, a simple shear model $\boldsymbol{F}_t = \boldsymbol{I} + \gamma_t(\eta)\boldsymbol{m}\otimes\boldsymbol{n}$ was utilized, where $\boldsymbol{F}_t$ is obviously non-symmetric. For martensitic variants, this corresponds to considering one of them as the reference configuration. This description is volume preserving, since $det\boldsymbol{F}_t = 1$. Using $\boldsymbol{m} = \boldsymbol{e}_2$ and $\boldsymbol{n} = \boldsymbol{e}_1$ for the sample considered in this paper, we calculate the transformation stretch tensor $\boldsymbol{U}_t = (\boldsymbol{F}_t^T \cdot \boldsymbol{F}_t)^{1/2}$ as

$$[\boldsymbol{U}_t] = \begin{bmatrix} (q_2q_4+q_3q_5)\Big/\left(2\sqrt{2}q_1\right) & (q_5-q_4)\Big/\left(\sqrt{2}q_1\right) & 0 \\ (q_5-q_4)\Big/\left(\sqrt{2}q_1\right) & (q_3q_4+q_2q_5)\Big/\left(2\sqrt{2}q_1\right) & 0 \\ 0 & 0 & 1 \end{bmatrix}, \tag{2.20}$$

where $q_1 = \sqrt{4+\gamma_t^2}$, $q_2 = q_1 - \gamma_t$, $q_3 = q_1 + \gamma_t$, $q_4 = \sqrt{2-q_2\gamma_t}$, and $q_5 = \sqrt{2+q_3\gamma_t}$. Note that U_{t12} and U_{t22} in Eq. (2.20) satisfy the equality $U_{t12}^2 + U_{t22}^2 = 1$, which as we will see, is a crucial condition for having a stress-free interface.

3. Analytical solution for an interface between martensitic variants in an infinite sample

3.1. Kinematic models I and II

We consider an infinite stress-free austenite sample, as depicted

in Fig. 1(a), as the reference body Ω_0. Let us apply transformation stretches U_{t1}^{ij} and U_{t2}^{ij} on the left and right sides of the reference sample about $\boldsymbol{e}_2$-axis, so that we obtain a fully twinned body consisting of variants M_1 and M_2. In a schematic of the deformed configuration with stationary distribution of η shown in Fig. 1(b), η varies between 0 and 1 within the interface and $\eta\to1$ and 0 in M_1 and M_2, respectively. All deformations are symmetric about the $\boldsymbol{e}_2$-axis, and for the zero external stresses the interface remains stationary. Furthermore, we assume that all fields are functions of r_{01} only (i.e., independent of r_{02}) and, thereby, reducing down the problem to one-dimensional (1D). This imposes the constraint

$$F_{12}=0 \quad \text{in the entire body.} \tag{3.1}$$

The solution of the Ginzburg-Landau equation (2.9) should asymptotically match with the solution in the bulk, which is the stress-free pure martensitic variants (see Ref. [75] for a similar treatment); i.e., η should satisfy the following boundary conditions:

$$\eta\to1 \text{ as } r_{01}\to-\infty, \text{ and } \eta\to0 \text{ as } r_{01}\to\infty. \tag{3.2}$$

Consequently,

$$U_{tij}\to U_{t1}^{ij} \text{ as } r_{01}\to-\infty, \text{ and } U_{tij}\to U_{t2}^{ij} \text{ as } r_{01}\to\infty. \tag{3.3}$$

Also, all the stresses are vanishing far away from the interface:

$$P_{11},P_{12},P_{21},P_{22},\sigma_{11},\sigma_{12},\sigma_{22}\to0 \text{ as } r_{01}\to\pm\infty. \tag{3.4}$$

Obviously, the elastic stretch $V_{eij}\to\delta_{ij}$:

$$V_{e11},V_{e22}\to1 \text{ and } V_{e12}\to0 \text{ as } r_{01}\to\pm\infty. \tag{3.5}$$

The stresses and strains are therefore now known in the bulk at $r_{01}\to\pm\infty$.

To obtain the solutions in the interface we will use the kinematic decomposition Eq. (2.1) and the compatibility condition Eq. (2.4). Also, we will consider that the entire sample is in mechanical equilibrium; hence the total traction at each cross-section of the sample parallel to $\boldsymbol{e}_2$-axis, and $\boldsymbol{e}_1$-axis are vanishing:

$$\int_{-\infty}^{\infty}\boldsymbol{P}\cdot\boldsymbol{e}_1\,dr_{02}=0 \text{ and } \int_{-\infty}^{\infty}\boldsymbol{P}\cdot\boldsymbol{e}_2\,dr_{01}=0, \tag{3.6}$$

at the respective cross-sections. Since P_{11} and P_{21} do not vary along $\boldsymbol{e}_2$ direction, they must vanish in the entire sample so that Eq. $(3.6)_1$ is respected:

$$P_{11}=P_{21}=0. \tag{3.7}$$

Using Eq. (3.1) and the relation $\boldsymbol{P}=J\boldsymbol{\sigma}\cdot\boldsymbol{F}^{-T}$ the components of first Piola-Kirchhoff stress tensor are obtained in terms of the Cauchy stresses as

$$\begin{aligned}P_{11}&=\frac{J\sigma_{11}}{F_{11}},\quad P_{12}=\frac{J}{F_{22}}\left(-\frac{\sigma_{11}F_{21}}{F_{11}}+\sigma_{12}\right),\\ P_{21}&=\frac{J\sigma_{12}}{F_{11}},\quad P_{22}=\frac{J}{F_{22}}\left(-\frac{\sigma_{12}F_{21}}{F_{11}}+\sigma_{22}\right).\end{aligned} \tag{3.8}$$

It is obvious from Eq. (3.8) that

$$\sigma_{11}=\sigma_{12}=P_{12}=0. \tag{3.9}$$

The solutions in Eq. (3.8) and Eq. (3.9) obviously satisfy the equilibrium equation (2.5). Considering Eq. (3.9) in Eq. $(3.6)_2$, we simplify it to

$$\int_{-\infty}^{\infty}P_{22}\,dr_{01}=0. \tag{3.10}$$

Calculating σ_{11} and σ_{12} using Eq. $(2.11)_1$ and then applying Eq. (3.9) we solve V_{e12} and V_{e11} which are given by Eqs. $(3.22)_2$ and $(3.22)_3$, respectively, in Box-I. It is to be mentioned that while solving $\sigma_{12}=0$, we obtained two other roots given by $V_{e12}=\pm\sqrt{(\lambda'+\mu)/(\lambda'+2\mu)-0.5(V_{e11}^2+V_{e22}^2)}$. However, assuming V_{e11} and V_{e22} are within 15% deviation from unity (even with such an assumption the magnitude of maximum stresses still can be several tens of GPa), one can easily verify that for NiAl, $(\lambda'+\mu)/(\lambda'+2\mu)=0.63$ (see Table 1 for material properties), and hence these roots are imaginary, and are not considered here.

Since the lattice rotation takes place about $\boldsymbol{e}_3$-axis, expressing R_{ij} as

$$R_{ij}=\begin{bmatrix}\cos\vartheta & -\sin\vartheta\\ \sin\vartheta & \cos\vartheta\end{bmatrix}, \tag{3.11}$$

and substituting Eq. (3.11) in Eq. (2.1) we obtain

$$\begin{aligned}&V_{e11}(U_{t11}\cos\vartheta-U_{t12}\sin\vartheta)=F_{11},\\ &V_{e11}(U_{t12}\cos\vartheta-U_{t22}\sin\vartheta)=F_{12}=0,\\ &V_{e22}(U_{t11}\sin\vartheta+U_{t12}\cos\vartheta)=F_{21},\\ &V_{e22}(U_{t12}\sin\vartheta+U_{t22}\cos\vartheta)=F_{22},\end{aligned} \tag{3.12}$$

where we have used Eqs. $(3.22)_2$ and (3.1). Since $V_{e11}\neq0$, Eq. $(3.12)_2$ yields

$$\begin{aligned}&\tan\vartheta=U_{t12}/U_{t22}\Rightarrow\sin\vartheta=U_{t12}\Big/\sqrt{U_{t12}^2+U_{t22}^2}, \text{ and}\\ &\cos\vartheta=U_{t22}\Big/\sqrt{U_{t12}^2+U_{t22}^2}.\end{aligned} \tag{3.13}$$

Substituting Eq. $(3.13)_{2,3}$ in Eq. (3.12) we obtain the total stretches:

$$\begin{aligned}&F_{11}=\frac{V_{e11}\left(U_{t11}U_{t22}-U_{t12}^2\right)}{\sqrt{U_{t12}^2+U_{t22}^2}},\quad F_{21}=\frac{V_{e22}U_{t12}(U_{t11}+U_{t22})}{\sqrt{U_{t12}^2+U_{t22}^2}}, \text{ and}\\ &F_{22}=V_{e22}\sqrt{U_{t12}^2+U_{t22}^2}.\end{aligned} \tag{3.14}$$

Since $\boldsymbol{F}$ is independent of r_{02} and r_{03}, and $F_{12}=F_{13}=F_{31}=F_{23}=F_{32}=0$, the compatibility condition (2.4) reduces to a single equation $\partial F_{22}/\partial r_{01}=0$. Hence by Eq. $(3.14)_3$ we have

$$F_{22}=V_{e22}\sqrt{U_{t12}^2+U_{t22}^2}=k_1=\sqrt{0.5\left(\alpha^2+\beta^2\right)}, \tag{3.15}$$

where k_1 is the integration constant. It is obtained from the condition that for $\eta\to1$ and $\eta\to0$, Eqs. (2.16) and (2.19) for KM-I and KM-II yield $U_{t12}^2+U_{t22}^2\to0.5(\alpha^2+\beta^2)$ and $V_{e22}\to1$ in those regions. Utilizing Eqs. (3.15), (2.16) and (2.19) in Eq. $(3.12)_4$ we obtain V_{e22} given by Eq. $(3.22)_{5,6}$ in Box-I. Eqs. $(3.22)_5$ and $(3.22)_6$ are the desired solutions for V_{e22} vs. $\phi[\eta(r_{01})]$ corresponding to KM-I and KM-II, which obviously approach unity as $r_{01}\to\pm\infty$. It is clear that they (and all the other fields) depend on the single parameter β/α, and for $\beta=\alpha$ one has $V_{e22}=1$ and that all strains and stresses are

zero. Using Eqs. $(3.22)_5$ and $(3.22)_6$ in combination with the interface profile $\eta(r_{01})$ for the chosen interpolation function $\phi(\eta)$ (see Eq. (3.27)), we obtain the spatial distribution of V_{e22}. Given V_{e22} by Eq. $(3.22)_5$ or $(3.22)_6$, we can now calculate V_{e11} using Eq. $(3.22)_3$, and V_{e33} using Eq. $(2.12)_1$. Finally, substituting Eq. $(3.22)_{2,3}$ in Eq. $(2.11)_1$, we obtain the desired σ_{22} as a function of V_{e22}:

$$\sigma_{22} = \frac{2\mu(\lambda'+\mu)V_{e22}\left(V_{e22}^2-1\right)}{2(\lambda'+\mu)-\lambda' V_{e22}^2}. \tag{3.16}$$

We can now substitute Eq. $(3.22)_5$ or $(3.22)_6$ and $(3.22)_3$ back into Eq. (3.14) to obtain the unknown components of the total deformation gradient F_{11}, F_{22}, and F_{21}. Since $V_{e22}\to 1$ in the bulk at $r_{01}\to\pm\infty$, we can easily verify from Eq. (3.16) that $\sigma_{22}\to 0$. Also, by Eq. (3.14), $F_{ij}\to R_{ik}U_{t1}^{kj}$ as $r_{01}\to -\infty$ and $F_{ij}\to R_{ik}U_{t2}^{kj}$ as $r_{01}\to\infty$ in the bulk. Components F_{e33} and F_{33} can be obtained using Eq. (2.12).

Stationary solution for Ginzburg-Landau equation.

It seems impossible to solve Eq. (2.9) for η analytically. However, we have estimated the order of magnitude of various terms in the Ginzburg-Landau equations and have shown that the transformation work related term can be neglected (see supplementary material [76]). Then the traditional solution [33,77] of Eq. (2.9) with the remaining terms is presented in Eq. $(3.27)_1$, where r_{0c} is the location within the interface where $\eta=0.5$, δ is the interfacial width (defined as the distance between points where $\eta=0.05$ and $\eta=0.95$), and γ is the interfacial energy.

Finally, all the solutions for the infinite sample are summarized in Box-I.

Interfacial force (tension) for KM-I

The resultant interfacial force, or interface tension is $f=\int_{-\infty}^{\infty}P_{22}dr_{01}$. Since P_{22} is highly nonlinear in η (compare with Eqs. (3.8) and (3.16)), the integration is performed using an approximate analytical expression for KM-I:

$$f=\frac{4\mu(\lambda'+\mu)}{\lambda'+2\mu}\int_{-\infty}^{\infty}g(\phi)dr_{01},\ \text{where} \tag{3.17}$$

$$g(\phi)=\frac{\sqrt{2\left(\alpha^2+\beta^2\right)}}{\alpha+\beta}\left[1-\frac{1}{2}\left(\frac{\alpha-\beta}{\alpha+\beta}\right)^2(1-2\phi)^2+\frac{3}{8}\left(\frac{\alpha-\beta}{\alpha+\beta}\right)^4(1-2\phi)^4\right]-1. \tag{3.18}$$

We obtained the integrand $g(\phi)$ in Eq. (3.17) by using Eq. $(3.22)_5$ in Eq. (3.16) and expanding it in the series of $(1-2\phi)^2(\beta-\alpha)^2/(\beta+\alpha)^2$, whose maximum value is $(\beta-\alpha)^2/(\beta+\alpha)^2\ll 1$ for NiAl (see Table 1). Using Eq. $(3.27)_{1,2}$ we calculate $\int_{-\infty}^{\infty}(1-2\phi)^2dr_{01}=0.5823\,\delta$ and $\int_{-\infty}^{\infty}(1-2\phi)^4dr_{01}=0.4530\,\delta$, and by substituting them in Eq. (3.17) we get the resultant interfacial force f (see Eq. $(3.28)_1$ in Box-I) which depends on the material constants. An important consequence of Eq. $(3.28)_1$ is that in the sharp interface limit, i.e. as $\delta\to 0$, the interfacial force also vanishes.

3.2. Kinematic model III

The transformation stretches given by Eq. (2.20) satisfy $U_{t12}^2+U_{t22}^2=1$. Hence, according to Eq. $(3.15)_{1,2}$, $V_{e22}=const$. Using Eq. (3.16) and the condition on σ_{22} in Eq. (3.4) we conclude that

$$V_{e22}=1\ \text{ and }\ \sigma_{22}=0\ \text{ in entire sample.} \tag{3.19}$$

Box-I

List of results for finite strain

1. Transformation stretches

$$\begin{aligned}
&U_{t11}=U_{t22}=0.5(\alpha+\beta)\ \text{ and }\ U_{t12}=0.5(\beta-\alpha)(1-2\phi)\ \text{ for KM}-\text{I};\\
&U_{t11}=U_{t22}=0.5\left(\alpha^{\phi}\beta^{1-\phi}+\alpha^{1-\phi}\beta^{\phi}\right)\ \text{ and }\ U_{t12}=0.5\left(\alpha^{\phi}\beta^{1-\phi}-\alpha^{1-\phi}\beta^{\phi}\right)\ \text{ for KM}-\text{II};\\
&U_{t11}=\frac{q_2q_4+q_3q_5}{2\sqrt{2}q_1},\ U_{t22}=\frac{q_3q_4+q_2q_5}{2\sqrt{2}q_1},\ \text{ and }\ U_{t12}=\frac{q_5-q_4}{\sqrt{2}q_1}\ \text{ for KM}-\text{III},
\end{aligned} \tag{3.20}$$

$$\text{where } q_1=\sqrt{4+\gamma_t^2}, q_2=q_1-\gamma_t, q_3=q_1+\gamma_t, q_4=\sqrt{2-q_2\gamma_t}, q_5=\sqrt{2+q_3\gamma_t}. \tag{3.21}$$

2. Lattice rotation and elastic stretches

$$\begin{aligned}
&\tan\vartheta=\frac{U_{t12}}{U_{t22}}\ \text{ and }\ V_{e12}=0\ \text{ for KM}-\text{I, II, III};\\
&V_{e11}=\sqrt{1-\frac{\lambda'\left(V_{e22}^2-1\right)}{\lambda'+2\mu}}\ \text{ for KM}-\text{I, II};\ \ V_{e11}=1\ \text{ for KM}-\text{III};\\
&V_{e22}=\frac{\sqrt{2\left(\alpha^2+\beta^2\right)}}{\sqrt{(\alpha+\beta)^2+(\alpha-\beta)^2(1-2\phi)^2}}\ \text{ for KM}-\text{I};\\
&V_{e22}=\frac{\sqrt{\alpha^2+\beta^2}}{\sqrt{\alpha^{2\phi}\beta^{2-2\phi}+\alpha^{2-2\phi}\beta^{2\phi}}}\ \text{ for KM}-\text{II};\\
&V_{e22}=1\ \text{ for KM}-\text{III};
\end{aligned} \tag{3.22}$$

$$V_{e22}^{max}=\frac{\sqrt{2\left(\alpha^2+\beta^2\right)}}{\alpha+\beta}\quad\text{for KM}-\text{I};\quad V_{e22}^{max}=\frac{\sqrt{\alpha^2+\beta^2}}{\sqrt{2\alpha\beta}}\quad\text{for KM}-\text{II}. \tag{3.23}$$

3. Total stretches

$$F_{11}=V_{e11}\frac{U_{t11}U_{t22}-U_{t12}^2}{\sqrt{U_{t12}^2+U_{t22}^2}},F_{22}=\sqrt{0.5\left(\alpha^2+\beta^2\right)},F_{12}=0,\ \text{and}$$
$$F_{21}=\frac{V_{e22}U_{t12}(U_{t11}+U_{t22})}{\sqrt{U_{t12}^2+U_{t22}^2}}\quad\text{for KM}-\text{I, II};\tag{3.24}$$
$$F_{11}=F_{22}=1,\quad F_{12}=0,\ \text{and}\quad F_{21}=\gamma_t\quad\text{for KM}-\text{III}.$$

4. The expressions for V_{e22}^2-1 and their maximum values:

$$V_{e22}^2-1=\frac{4(\alpha-\beta)^2\phi(1-\phi)}{(\alpha+\beta)^2+(\alpha-\beta)^2(1-2\phi)^2},\quad max\left(\left|V_{e22}^2-1\right|\right)=\frac{(\alpha-\beta)^2}{(\alpha+\beta)^2}\quad\text{for KM}-\text{I};$$
$$V_{e22}^2-1=\frac{\alpha^2+\beta^2-\alpha^{2\phi}\beta^{2-2\phi}-\alpha^{2-2\phi}\beta^{2\phi}}{\alpha^{2\phi}\beta^{2-2\phi}+\alpha^{2-2\phi}\beta^{2\phi}},\quad max\left(\left|V_{e22}^2-1\right|\right)=\frac{(\alpha-\beta)^2}{2\alpha\beta}\quad\text{for KM}-\text{II}.\tag{3.25}$$

5. Cauchy stresses

$$\sigma_{11}=\sigma_{12}=0\quad\text{for KM}-\text{I, II, III};$$
$$\sigma_{22}=\frac{2\mu(\lambda'+\mu)V_{e22}\left(V_{e22}^2-1\right)}{2(\lambda'+\mu)-\lambda'V_{e22}^2}\quad\text{for KM}-\text{I, II; and }\sigma_{22}=0\ \text{for KM}-\text{III}.\tag{3.26}$$

6. Order parameter, interpolation function, interface width and energy

$$\eta=1/(1+\exp[-6(r_{01}-r_{0c})/\delta]);\quad \phi=\eta^2(3-2\eta);\quad \delta=\sqrt{18b/A};\quad \gamma=b/\delta.\tag{3.27}$$

7. Resultant interfacial force

$$f=\tilde{f}\,\delta,\quad\text{for KM}-\text{I},\quad\text{and}\quad f=0\quad\text{for KM}-\text{III, where}\tag{3.28}$$

$$\tilde{f}=\frac{4\mu(\lambda'+\mu)}{\lambda'+2\mu}\left[\frac{\sqrt{2\left(\alpha^2+\beta^2\right)}}{\alpha+\beta}\left\{1-0.2912\left(\frac{\alpha-\beta}{\alpha+\beta}\right)^2+0.1699\left(\frac{\alpha-\beta}{\alpha+\beta}\right)^4\right\}-1\right].\tag{3.29}$$

Since all stresses are zero within the sample, the resultant force f defined in Eq. (3.17) is zero as well. Results are listed in Box-I for finite deformation and in Box-II for small strains. Some other arguments are given in Ref. [30].

Although, $\boldsymbol{U}_t$ given by Eq. (2.20) successfully describes a stress-free twinning solution, there are several difficulties in using it for a more general study: (i) For multivariant PTs, it is not trivial to include simple shear transformations between all variants. In particular, each pair of twin-related variants has two possible twin parameters $\boldsymbol{n}$ and $\boldsymbol{m}$; the number of order parameters hence will be doubled. Also, a proper orientation of variants should be provided. Also, relation (2.20) is for a plane interface, and it is not clear how to treat curved interfaces. (ii) Not all martensitic variants in a material are in twin relationship (e.g., for cubic to monoclinic transformation); hence the transformation rule (2.20) cannot be applied to all martensitic transformations.

Table 1
List of parameters for NiAl.

Parameter	Value	reference
λ	74.62 GPa	[4]
μ	72 GPa	[4]
α	0.922	[4]
β	1.215	[4]
γ	0.05 J/m^2	typical (see e.g. Ref. [38])
δ	0.75 nm	
A	1.2 GPa	using Eq. $(3.27)_3$
b	3.75×10^{-11} N	using Eq. $(3.27)_4$

3.3. Small strain approximation

Under small strain and rotation assumption, $|\varepsilon_{ij}|\ll1$, $|\varepsilon_{tij}|\ll1$, $|\varepsilon_{eij}|\ll1$, $|F_{21}|\ll1$, and $|\vartheta|\ll1$. Expanding all the equations in Box-I into Taylor's series about strain-free state we obtain the results in Box-II. For small strains, the transformation strains for KM-I and KM-II coincide (see Eq. (3.30)). Lattice rotation is proportional to $\varepsilon_{t1}-\varepsilon_{t2}$ and the normal elastic strains and stresses are proportional to $(\varepsilon_{t1}-\varepsilon_{t2})^2$, i.e., they are square of the difference in transformation strains (see Eq. (3.31)), where $\varepsilon_{t1}=\alpha-1$ and $\varepsilon_{t2}=\beta-1$.

Box-II
List of results for small strain

1. Transformation strains

$$\varepsilon_{t11}=\varepsilon_{t22}=0.5(\varepsilon_{t1}+\varepsilon_{t2}) \quad \text{and} \quad \varepsilon_{t12}=0.5(\varepsilon_{t2}-\varepsilon_{t1})(1-2\phi) \quad \text{for KM}-\text{I, II;}$$
$$\varepsilon_{t11}=\varepsilon_{t22}=0 \quad \text{and} \quad \varepsilon_{t12}=0.5\gamma_t \quad \text{for KM}-\text{III;} \tag{3.30}$$

2. Lattice rotation and elastic strains

$$\vartheta=0.5(\varepsilon_{t2}-\varepsilon_{t1})(1-2\phi) \quad \text{for KM}-\text{I, II;} \quad \vartheta=0.5\gamma_t \quad \text{for KM}-\text{III}$$
$$\varepsilon_{e12}=0, \quad \varepsilon_{e11}=-\frac{\lambda'\phi(1-\phi)(\varepsilon_{t1}-\varepsilon_{t2})^2}{2(\lambda'+2\mu)}, \quad \text{and} \quad \varepsilon_{e22}=\frac{1}{2}\phi(1-\phi)(\varepsilon_{t1}-\varepsilon_{t2})^2 \quad \text{for KM}-\text{I;}$$
$$\varepsilon_{e12}=0, \quad \varepsilon_{e11}=-\frac{\lambda'\phi(1-\phi)(\varepsilon_{t1}-\varepsilon_{t2})^2}{\lambda'+2\mu}, \quad \text{and} \quad \varepsilon_{e22}=\phi(1-\phi)(\varepsilon_{t1}-\varepsilon_{t2})^2 \quad \text{for KM}-\text{II;} \tag{3.31}$$
$$\varepsilon_{e12}=\varepsilon_{e11}=\varepsilon_{e22}=0 \quad \text{for KM}-\text{III.}$$

3. Total strains

$$\varepsilon_{11}=\varepsilon_{e11}+0.5(\varepsilon_{t1}+\varepsilon_{t2}), \quad \varepsilon_{22}=0.5(\varepsilon_{t1}+\varepsilon_{t2}), \quad \text{and} \quad \varepsilon_{12}=0.5(\varepsilon_{t1}+\varepsilon_{t2})(1-2\phi) \quad \text{for KM}-\text{I, II;}$$
$$\varepsilon_{11}=\varepsilon_{22}=0 \quad \text{and} \quad \varepsilon_{12}=0.5\gamma_t \quad \text{for KM}-\text{III.} \tag{3.32}$$

4. Cauchy stresses

$$\sigma_{11}=\sigma_{12}=0 \quad \text{for KM}-\text{I, II;} \quad \sigma_{22}=\frac{2\mu(\lambda'+\mu)}{\lambda'+2\mu}\phi(1-\phi)(\varepsilon_{t1}-\varepsilon_{t2})^2 \quad \text{for KM}-\text{I;}$$
$$\sigma_{22}=\frac{4\mu(\lambda'+\mu)}{\lambda'+2\mu}\phi(1-\phi)(\varepsilon_{t1}-\varepsilon_{t2})^2 \quad \text{for KM}-\text{II;} \tag{3.33}$$
$$\sigma_{11}=\sigma_{12}=\sigma_{22}=0 \quad \text{for KM}-\text{III.}$$

5. Resultant interfacial force

$$f=\tilde{f}\,\delta \quad \text{for KM}-\text{I,} \quad \text{and} \quad f=0 \quad \text{for KM}-\text{III, where} \quad \tilde{f}=\frac{0.2088\mu(\lambda'+\mu)}{\lambda'+2\mu}(\varepsilon_{t2}-\varepsilon_{t1})^2. \tag{3.34}$$

For small strains, the interface stress for KM-II is twice that which corresponds to KM-I (see Eq. (3.33)). An estimation for the interface force is given by Eq. (3.34). For KM-III, only ε_{t12} is non-trivial, which is listed in Eq. (3.30). All elastic strains are vanishing, and so are the stresses and the interface force (see Eqs. (3.31), (3.33) and (3.34)). Normal components of the total strain are zero, and the shear component is same as ε_{t12} (see Eq. (3.32)).

3.4. Discussion

It is thus clear from Eq. (3.15), which is obtained from the strain compatibility relation, that the constitutive relations for $\boldsymbol{U}_t$ given by Eqs. (2.16) and (2.19) are not compatible with unit elastic stretch V_{22} (or equivalently, vanishing elastic strains) across the twin boundary. Such incompatibility is accommodated by the large elastic stress σ_{22} in the twin boundary. Our analytical treatment in a twinned sample has clearly shown the reason for elastic stresses in a diffused twin boundary in phase field studies in Refs. [30,38,39] and has quantified them.

We now present a detailed quantitative analysis showing the non-trivial stresses and strains. We have plotted only the non-trivial components of stress, lattice rotation, and other strains ε_{ij}, ε_{tij}, and ε_{eij} (see Eq. (2.3) for their definitions) along the line $r_{02}=0$ in Ω_0. Results for NiAl have been presented. The material parameters are listed in Table 1.

In Fig. 2(a) ε_{e11} and ε_{e22} are compared for $\boldsymbol{U}_t$ given by models KM-I and KM-II. Normal elastic strains within the interface are larger for KM-II compared to those for KM-I. Fig. 2(b) shows that σ_{22} for both models reaches several GPa; that is to say, it is quite large. The maximum value of the elastic strain and stress is attained at the middle of the interface where $\eta=0.5$ (compare with Eqs. $(3.25)_{2,4}$, (3.23), $(3.26)_2$, and $(3.27)_1$ in Box-I). The ratio of V_{e22} for those two models at $\eta=0.5$ is $V^{\mathrm{II}}_{e22}/V^{\mathrm{I}}_{e22}=0.5(\alpha+\beta)/\sqrt{\alpha\beta}$, which is always greater than unity for all positive $\alpha\neq\beta$. Consequently, the maximum stress (calculated at $\eta=0.5$) is also larger for KM-II. We have shown the variation of maximum stress (non-dimensionalized by μ) with the stretch ratio β/α for both the models in Fig. 2(c). For all β/α, $\max(\sigma^{\mathrm{II}}_{22})\geq 2\max(\sigma^{\mathrm{I}}_{22})$, and the maximum stress ratio

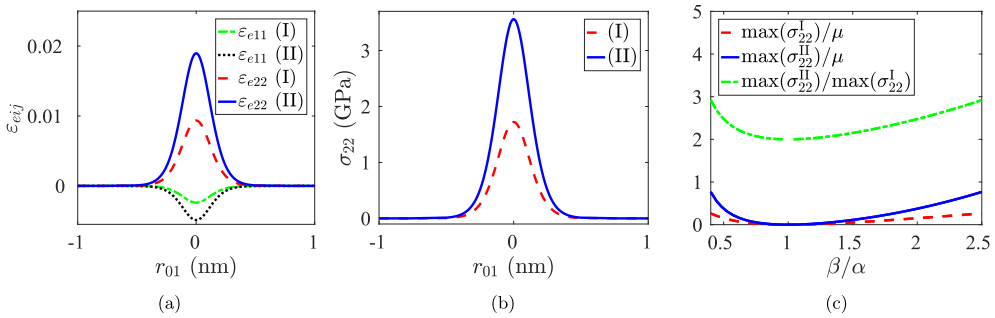

Fig. 2. Plots for infinite sample: (a) ε_{e11} and ε_{e22}, and (b) stress σ_{22}; (c) variation of max $(\sigma_{22})/\mu$ at the mid point of the interface where $\eta = 0.5$ for KM-I and KM-II. In the legends 'I' and 'II' indicate KM-I and KM-II, respectively.

approaches 2 as $\beta/\alpha \to 1$. It should be mentioned that the net elastic energy stored within the interface per unit area of the cross-section of the reference sample perpendicular to $\boldsymbol{e}_1$-axis, i.e. $\int_{-\infty}^{\infty} J_t \overline{\psi}_e dr_{01}$ has been calculated to be 1.7×10^{-3} J/m^2 for KM-I and 6.8×10^{-3} J/m^2 for KM-II, where $\overline{\psi}_e$ is given by Eq. (2.7). This energy is obviously much smaller than the structural energy of the interface $\gamma = 0.05$ J/m^2. This means that the elastic stresses defined in the paper and corresponding resultant force are not described by the second term $\partial\gamma/\partial\varepsilon_i$ in the Shuttleworth equation [20] but related to the heterogeneity of the transformation strain within a finite-width interface. Since these stresses are independent of the interface width, for a sharp interface the resultant force $f = 0$.

Variations of the components of ε_{tij}, ε_{ij}, and $\tan\vartheta$ are shown in Fig. 3. In some of the plots the components have been scaled up for better readability. The component $\varepsilon_{t11} = \varepsilon_{t22}$ is constant everywhere for KM-I. However, for KM-II we see that it decreases within the interface, which can be easily explained by looking at $det\, \boldsymbol{U}_t = (U_{t11}^2 - U_{t12}^2)\alpha = \text{const.}$, as shown in Eq. (2.18), where we have considered $U_{t11} = U_{t22}$ and $U_{t33} = \alpha$. Since U_{t12} is heterogeneous across the interface, U_{t11} and U_{t22} also must vary appropriately to maintain the constancy of $det\, \boldsymbol{U}_t$. Variations of the components of ε_{ij} are shown in Fig. 3(b). Since ε_{22} for both models are identical constants (see Eq. (3.15)), just a single curve has been shown. The other components $3\varepsilon_{11}$ and F_{21} vary heterogeneously across the interface. Plots for $\tan\vartheta$ are shown in Fig. 3(c); for both models they are almost coincident.

4. Analytical and FE solutions for an interface between martensitic variants in a finite sample

We will now consider a finite sample, which is more realistic configuration, to show the effect of external surfaces on stresses and strains. A stress-free austenite sample is considered as the reference body (see the shape in Fig. 4(a)). We denote the width (along $\boldsymbol{e}_1$ direction) of the reference sample by $w \gg \delta$. The following boundary conditions for the mechanics problem are assumed: all external surfaces are traction-free; the bottom-left corner point is fixed, and $\boldsymbol{e}_1$ component of displacement at left surface is zero. The reference sample is deformed to obtain a twinned body in a way similar to how it was obtained in the infinite sample. Here the deformed sample is rectangular (see Fig. 4(b)). An approximate analytical solution for KM-I has been derived and compared with FE results. Numerical solution have been presented for KM-II and compared with the results for KM-I.

4.1. Analytical treatment for KM-I

We utilize the St. Venant principle and restrict our analysis to the region away from the upper and lower free surfaces. We assume that in that region the solutions are independent of r_{02} and are functions of r_{01} only. Hence the condition (3.1) $F_{12} = 0$ is valid in that region. Repeating the same steps as for an infinite sample, we see that the expressions for elastic stretches V_{e11} and V_{e12}, total stretches F_{11}, F_{21}, and F_{22}, lattice rotation ϑ, stresses $P_{11} = P_{12} = P_{21} = \sigma_{11} = \sigma_{12} = 0$, and σ_{22} for finite sample are identical to those obtained for the infinite sample listed in Box-I. The force equilibrium condition (see Eq. (3.6))

$$\int_{-w/2}^{w/2} P_{22} dr_{01} = 0 \tag{4.1}$$

must be satisfied at each cross-section along the width of the sample. This condition will determine V_{e22} for a finite sample. Once V_{e22} is known, all other solutions can be easily computed. For the finite sample we consider that stationary η is given by Eq. $(3.27)_1$. Since $w \gg \delta$, the stresses and strains within the finite sample differ slightly from that in the infinite sample, and do not affect η.

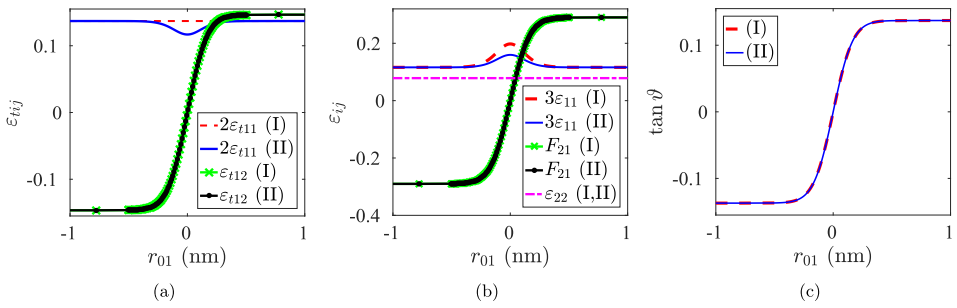

Fig. 3. Plot for infinite sample: (a) $2\varepsilon_{t11}$ $(= 2\varepsilon_{t22})$ and ε_{t12}; (b) $3\varepsilon_{11}$, F_{21}, and ε_{22}; (c) $\tan\vartheta$.

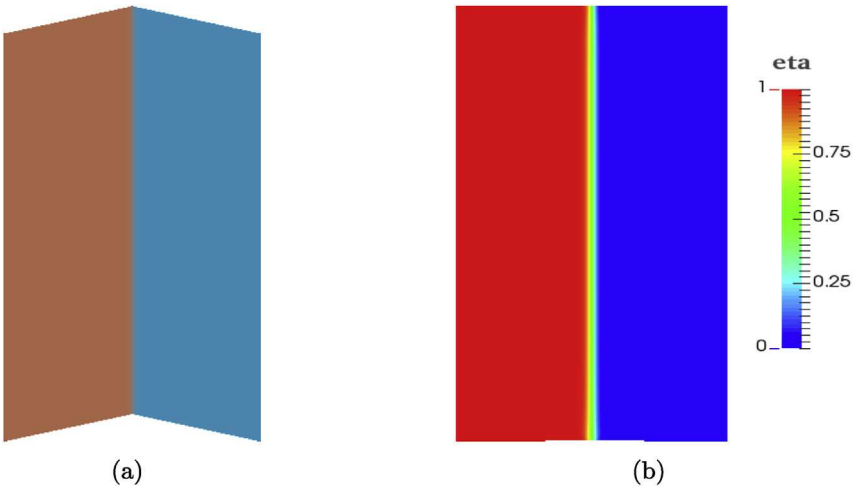

Fig. 4. Finite sample geometry with distribution of η in FE computations: (a) initial stress-free reference configuration of A; (b) twinned sample (deformed configuration) with stationary distribution of η.

Let us now determine σ_{22} and V_{e22}. We have seen that for an infinite sample, σ_{22} within the interface is tensile (see Fig. 2(b)). Hence we expect that for a finite sample, the force equilibrium at the cross-section along the width of the sample would require that the bulk to be under compression. Since we consider $w \gg \delta$, the magnitude of σ_{22} outside the interface will be much smaller than σ_{22}^{max} within the interface. We therefore assume that σ_{22} in the bulk is constant (denoted by Σ), and σ_{22}^{w} for the finite sample is equal to σ_{22}^{∞} in infinite sample superposed by Σ, i.e.

$$\sigma_{22}^{w} = \sigma_{22}^{\infty} + \Sigma. \tag{4.2}$$

Both σ_{22}^{w} and σ_{22}^{∞} have the same expression given by Eq. $(3.26)_2$, but, V_{e22} are different in these samples. In the infinite sample V_{e22} is given by Eq. $(3.22)_{5,6}$ for KM-I and KM-II, respectively, and in the finite sample it is yet to be determined. Since $\sigma_{22}^{\infty} = 0$ outside the interface, using Eq. (4.2) we can rewrite the force equilibrium condition Eq. (4.1) as

$$\int_{-\delta/2}^{\delta/2} J\sigma_{22}^{\infty} dr_{01} + \sum \int_{-w/2}^{w/2} J dr_{01} = 0, \tag{4.3}$$

where we have used Eq. $(3.8)_4$ and $F_{22} = const$. The integral in Eq. (4.3) is not analytically tractable when σ_{22} given by Eq. $(3.26)_2$. If we assume $J \approx const$, we note that the integral has already been evaluated in Eq. (3.29) (for KM-I), which can be used here to obtain $\Sigma \approx -f/w$. Hence we have

$$\sigma_{22}^{w} = \sigma_{22}^{\infty} - (\delta/w)\tilde{f}, \tag{4.4}$$

where σ_{22}^{∞} is evaluated using V_{e22}^{∞} given by Eq. $(3.22)_5$ for the infinite sample, and we have used Eq. (3.28). Then in principle, using Eq. $(3.26)_3$ in Eq. (4.4) for σ_{22}^{w} we can calculate V_{e22}^{w} for the finite sample. Alternatively, we obtain an approximate solution for V_{e22}^{w} as follows. We know that $\sigma_{22}^{\infty} = 0$ in the bulk and $|\Sigma| = |f/w| \ll \sigma_{22}^{max}$, we infer that V_{e22} in the bulk deviates slightly from unity. Then defining

$$V_{e22}^{w} = V_{e22}^{\infty} + \chi, \quad \text{where} \quad |\chi| \ll 1, \tag{4.5}$$

we use it in Eq. (4.4) away from the interface (where $V_{e22}^{\infty} = 1$) and linearize it about $\chi = 0$ to obtain

$$\chi = -\frac{f(\lambda' + 2\mu)}{4w\mu(\lambda' + \mu)}. \tag{4.6}$$

Now, we compare the bulk stress with the maximum value of the stress within the interface for KM-I. We approximately evaluate the maximum stress in the finite sample by considering $\eta = 0.5$ in Eq. (4.4) as

$$\max\left(\sigma_{22}^{I}\right) = \frac{4\mu(\lambda' + \mu)}{\lambda' + 2\mu}\left(\frac{\sqrt{2\left(\alpha^2 + \beta^2\right)}}{\alpha + \beta} - 1\right). \tag{4.7}$$

Hence the ratio of bulk stress and the maximum stress in the interface can be expressed as

$$\frac{\Sigma}{\max(\sigma_{22}^{I})} = -\frac{\delta}{w}\frac{\left(\sqrt{2\left(\alpha^2 + \beta^2\right)}\Big/(\alpha + \beta)\right)\left\{1 - 0.2912(\alpha - \beta)^2\Big/(\alpha + \beta)^2 + 0.1699(\alpha - \beta)^4\Big/(\alpha + \beta)^4\right\} - 1}{\left(\sqrt{2\left(\alpha^2 + \beta^2\right)}\Big/(\alpha + \beta)\right) - 1}. \tag{4.8}$$

In summary, V_{e22}^{w} in finite sample can be obtained using Eqs. (4.5) and (4.6); σ_{22}^{w} is calculated using Eq. (4.4), where σ_{22}^{∞} is given by Eq. $(3.26)_2$; all other stresses, rotation, and stretches are identical to those listed in Box-I, where V_{e22} therein is for the infinite sample.

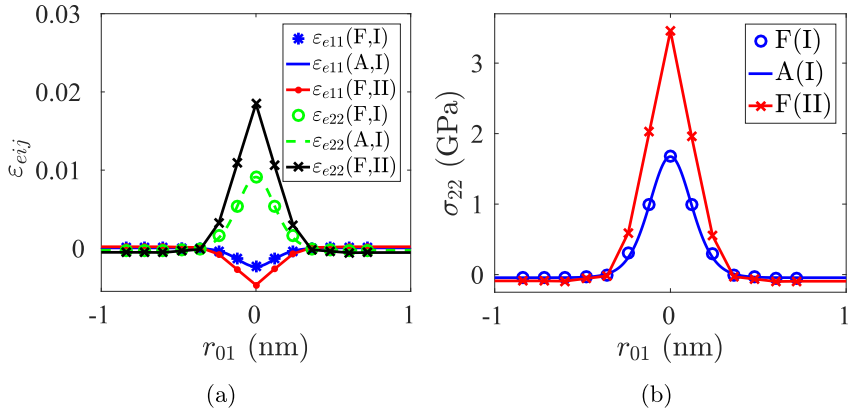

Fig. 5. Plots for finite sample along $r_{02} = 0$ for KM-I and II: (a) ε_{e11} and ε_{e22}; (b) σ_{22}. In legend, 'A' and 'F' stand for analytical and FE results, respectively.

4.2. Discussions on analytical and FE results

We will analyze the following results: for KM-I both analytical (derived in Section 4.1) and FE results, and for KM-II FE results only will be discussed. For FE simulations, a 12 nm wide and 24 nm long (length along any cross-section in $\boldsymbol{e}_2$ direction) sample (Ω_0), as shown in Fig. 4(a), has been discretized uniformly with 2160 fourth order quadrilateral elements. The total degrees of freedom is 104835. Displacement and traction boundary conditions, as outlined in the beginning of the subsection, have been applied. FE computations have been carried out using an open source deal.II library [78], where we have written a nonlinear FE code for solving the coupled mechanics and phase field equations. Detailed computational algorithm will be presented elsewhere. The deformed body with the stationary η is shown in Fig. 4(b). The interface profile obtained using FE computation matches with the stress-independent analytical solution given by Eq. $(3.27)_1$, and the interface width is 0.75 nm. The results shown in Figs. 5 and 6 have been plotted along $r_{02} = 0$ line in Ω_0, which obviously passes through the middle of the sample. For better readability of the data, all plots are shown for -1 nm $\leq r_{01} \leq 1$ nm. Analytical and numerical results for elastic stretches and stress σ_{22} are compared in Fig. 5(a) and (b), respectively, for both KM-I and II. FE and analytical solutions for KM-I are in a good agreement. The results within the twin boundary are qualitatively similar to those obtained for infinite sample. However, within bulk, elastic stretches are less than unity, and the stress σ_{22} is compressive, which balances the tensile force generated within the twin boundary for accommodating the incompatibility. Various components of ε_{tij}, ε_{ij}, F_{ij}, and $\tan\vartheta$, shown in Fig. 6(a), (b), and (c), are qualitatively similar to those for an infinite sample.

5. Concluding remarks

In the sharp interface approach, the boundary between two martensitic variants, which are in a twin relationship, is stress-free, i.e., it does not generate elastic stresses because of the lack of lattice incompatibility. However, in the phase field approach, a finite width interface generates elastic stresses [4,33,38,39], but the reason was unclear. There had been only limited attempts to find out which parameters affect elastic interfacial stresses for solid-solid interface and how they can be controlled. Here, the origin of a large elastic stress within an interface between martensitic variants (twins) within a finite strain phase field approach has been determined by obtaining an analytical finite-strain solution for an infinite sample. Example with cubic austenite and tetragonal martensite has been treated under plane stress condition. Three different constitutive relations for the transformation stretch tensor versus order parameters have been considered: (a) a linear combination (KM-I) of the Bain tensors for the martensitic variants [30,67]; (b) an exponential-logarithmic combination (KM-II) of the Bain tensors [38,39], which preserves volume for any intermediate state along the transformation path between martensitic variants; and (c) simple shear (KM-III) in one variant with respect to another [40,64,71]. Stresses are absent for KM-III, but it is unclear how to generalize this model for a multivariant martensitic transformation. The first two models generate elastic stresses within the interface, which are along the interface, because of the variable component of the transformation deformation gradient along the interface normal. Stress distribution depends on the interpolation function for the transformation deformation gradient $\phi(\eta)$ and r_{01}/δ, and resultant force per unit interface length f (surface tension) is proportional to the interface width δ. Thus, for the sharp

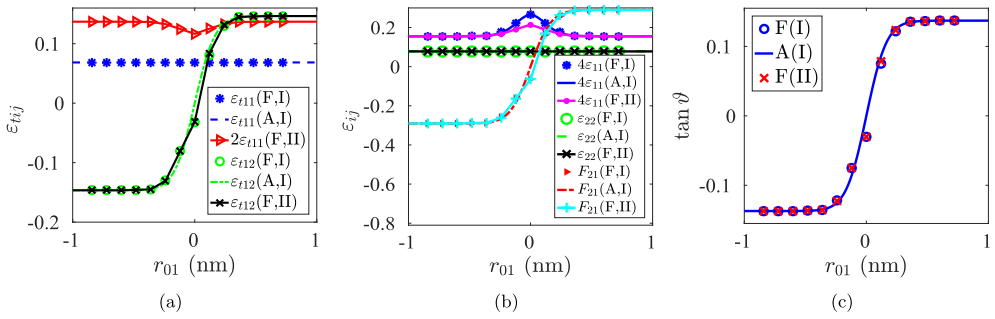

Fig. 6. Plots for finite sample along $r_{02} = 0$ for KM-I and II; (a) ε_{t11}, and ε_{t12}; (b) ε_{11}, F_{21}, and ε_{22}; (c) $\tan\vartheta$. In legend, 'A' and 'F' mean analytical and FE results, respectively.

interface surface tension is zero. However, for an alternating twin structure with a traditional several nanometers spacing between interfaces [70], comparable with the finite interface width, the effect of surface tension can be significant. The magnitude of the interfacial stresses for NiAl alloy is several GPa, which is significantly large. The maximum interfacial stress for KM-II is more than twice that which corresponds to KM-I.

Note that for small transformation strains, expressions for the transformation deformation gradient for KM-I and KM-II coincide, and the lattice rotation and stress are proportional to $(\varepsilon_{t1}-\varepsilon_{t2})^2$, meaning they are higher order terms. Even for small strains, the interface stress for KM-II is double that which corresponds to KM-I.

An approximate analytical solution for a finite sample has also been found. It contains small compressive stresses in bulk to equilibrate tensile interface tension. The analytical solution is in good correspondence with numerical results obtained using the FE method.

The main question is whether elastic interfacial stresses are real or just an artifact of the model. The magnitude of the interfacial stresses within a twin interface should be determined with the help of atomistic simulations, similar to [1,16,17] for other interfaces. Then the difference between the atomistic results and the structural stresses σ_{st} will represent elastic stresses. Intuitively, stresses obtained here are too high for both KM-I and KM-II. From this point of view, KM-I is better that KM-II, and also simpler. The requirement of volume preservation during twinning is plausible but not mandatory. There are data indicating that that dislocational slip is also not isochoric process between two stable atomic configurations [68]. Also, other defects such as stacking fault and twin boundaries may induce volume change (Chapter 7 and 8 of [69] and references therein).

On the other hand, based on the parameter values for NiAl, the interfacial force f is estimated to be 0.6 N/m for KM-I, and 1.2 N/m for KM-II. To the best of our knowledge, there is no experimental data or atomistic simulations for the interfacial stresses for twin interface. However, there are estimation for f for the external surfaces of nanowires [1], which was in the range of 1–3.5 N/m. The variant-variant interfacial stresses are expected to be smaller than the stresses within external surfaces. Hence our interfacial stress values are reasonable and should be close to reality.

The obtained results also demonstrate that the requirements of the phase field theories should be formulated not only for conditions when one phase homogeneously transforms into another one, but also for the case with coexistence of both phases divided by an interface. That is why the obtained results are important for developing phase field approaches for multivariant martensitic PTs coupled to mechanics, especially at the nanoscale.

Acknowledgments

Support of NSF (CMMI-1536925 and DMR-1434613), ARO (W911NF-17-1-0225), ONR (N00014-16-1-2079), and Iowa State University (Schafer 2050 Challenge Professorship) is gratefully acknowledged. Simulations were performed at Extreme Science and Engineering Discovery Environment (XSEDE), allocations TG-MSS140033 and MSS170015.

Appendix A. Supplementary data

Supplementary data related to this article can be found at http://dx.doi.org/10.1016/j.actamat.2017.07.059.

References

[1] J. Diao, K. Gall, M.L. Dunn, Surface-stress-induced phase transformation in metal nanowires, Nat. Mater. 2 (2003) 656–660.
[2] S. Li, X. Ding, J. Li, X. Ren, J. Sun, E. Ma, T. Lookman, Inverse martensitic transformation in Zr nanowires, Phys. Rev. B 81 (2010) 245433.
[3] V.I. Levitas, M. Javanbakht, Surface tension and energy in multivariant martensitic transformations: phase-field theory, simulations, and model of coherent interface, Phys. Rev. Lett. 105 (2010) 165701.
[4] V.I. Levitas, M. Javanbakht, Phase-field approach to martensitic phase transformations: effect of martensite-martensite interface energy, Int. J. Mater. Res. 102 (2011) 652–665.
[5] K. Momeni, V.I. Levitas, J.A. Warren, The strong influence of internal stresses on the nucleation of a nanosized, deeply undercooled melt at a solid-solid interface, Nano Lett. 15 (2015) 2298–2303.
[6] J. Luo, Developing interfacial phase diagrams for applications in activated sintering and beyond: current status and future directions, J. Am. Ceram. Soc. 95 (2012) 2358–2371.
[7] P.R. Cantwell, M. Tang, S.J. Dillon, J. Luo, G.S. Rohrer, M.P. Harmer, Grain boundary complexions, Acta Mater. 62 (2014) 1–48.
[8] J. Luo, H. Cheng, K.M. Asl, C.J. Kiely, M.P. Harmer, The role of a bilayer interfacial phase on liquid metal embrittlement, Science 333 (2011) 1730–1733.
[9] S.J. Dillon, M. Tang, W.C. Carter, M.P. Harmer, Complexion: a new concept for kinetic engineering in materials science, Acta Mater. 55 (2007) 6208–6218.
[10] V.I. Levitas, B.F. Henson, L.B. Smilowitz, B.W. Asay, Solid-solid phase transformation via virtual melt, significantly below the melting temperature, Phys. Rev. Lett. 92 (2004) 235702.
[11] V.I. Levitas, B.F. Henson, L.B. Smilowitz, B.W. Asay, Solid-solid phase transformation via internal stress-induced virtual melting, significantly below the melting temperature. Application to HMX energetic crystal, J. Phys. Chem. B 110 (2006) 10105–10119.
[12] V.I. Levitas, Crystal-amorphous and crystal-crystal phase transformations via virtual melting, Phys. Rev. Lett. 95 (2005) 075701.
[13] S.L. Randzio, A. Kutner, Metastability and instability of organic crystalline substances, J. Phys. Chem. B 112 (2008) 1435–1444.
[14] V.I. Levitas, Z. Ren, Y. Zeng, Z. Zhang, G. Han, Crystal-crystal phase transformation via surface-induced virtual premelting, Phys. Rev. B 85 (2012) 220104.
[15] Y. Peng, F. Wang, Z. Wang, A.M. Alsayed, Z. Zhang, A.G. Yodh, Y. Han, Two-step nucleation mechanism in solid-solid phase transitions, Nat. Mater. 14 (2015) 101–108.
[16] T. Frolov, Y. Mishin, Orientation dependence of the solid-liquid interface stress: atomistic calculations for copper, Model. Simul. Mater. Sci. Eng. 18 (2010) 074003.
[17] T. Frolov, Y. Mishin, Effect of nonhydrostatic stresses on solid-fluid equilibrium. II. Interface thermodynamics, Phys. Rev. B 82 (2010) 174114.
[18] T. Frolov, Y. Mishin, Thermodynamics of coherent interfaces under mechanical stresses, I. Theory, Phys. Rev. B 85 (2012) 224106.
[19] J.W. Gibbs, The Collected Works of J. Willard Gibbs, Yale University Press, New Haven, 1948.
[20] F.D. Fischer, T. Waitz, D. Vollath, N.K. Simha, On the role of surface energy and surface stress in phase-transforming nanoparticles, Prog. Mat. Sci. 53 (2008) 481–527.
[21] J.W. Cahn, Theromodynamics of solid and fluid surfaces, in: W.C. Johnson, J.M. Blackely (Eds.), Interface Segregation, American Society of Metals, Metals Park, OH, 1979, pp. 3–23. Chap. 1.
[22] I.S. Podstrigach, I.Z. Povstenko, Introduction in Mechanics of Surface Phenomena in Deformable Solids, Naukova Dumka, Kiev, 1985.
[23] M.E. Gurtin, A. Struthers, Multiphase thermomechanics with interfacial structure 3. Evolving phase boundaries in the presence of bulk deformation, Arch. Ration. Mech. Anal. 112 (1990) 97–160.
[24] Y.Z. Povstenko, Generalizations of Laplace and Young equations involving couples, J. Colloid Interf. Sci. 144 (1991) 497–506.
[25] M.E. Gurtin, A.I. Murdoch, A continuum theory of elastic material surfaces, Arch. Ration. Mech. Anal. 57 (1975) 291–323.
[26] A. Javili, P. Steinmann, On thermomechanical solids with boundary structures, Int. J. Solids Struct. 47 (2010) 3245–3253.
[27] H.L. Duan, J. Wang, B.L. Karihaloo, Theory of elasticity at the nanoscale, Adv. Appl. Mech. 42 (2009) 1–68.
[28] V.I. Levitas, D.W. Lee, Athermal resistance to interface motion in the phase-field theory of microstructure evolution, Phys. Rev. Lett. 99 (2007) 245701.
[29] A.V. Idesman, J.Y. Cho, V.I. Levitas, Finite element modeling of dynamics of martensitic phase transitions, Appl. Phys. Lett. 93 (2008) 043102.
[30] V.I. Levitas, A.M. Roy, D.L. Preston, Multiple twinning and variant-variant transformations in martensite: phase-field approach, Phys. Rev. B 88 (2013) 054113.
[31] V.I. Levitas, V.A. Levin, K.M. Zingerman, E.I. Freiman, Displacive phase transitions at large strains: phase-field theory and simulations, Phys. Rev. Lett. 103 (2009) 025702.
[32] V.A. Levin, V.I. Levitas, K.M. Zingerman, E.I. Freiman, Phase-field simulation of stress-induced martensitic phase transformations at large strains, Int. J. Solids Struct. 50 (2013) 2914–2928.
[33] V.I. Levitas, A.M. Roy, Multiphase phase field theory for temperature- and stress-induced phase transformations, Phys. Rev. B 91 (2015) 174109.
[34] C.H. Lei, L.J. Li, Y.C. Shu, J.Y. Li, Austenite-martensite interface in shape memory alloys, Appl. Phys. Lett. 96 (2010) 141910.
[35] Y.M. Jin, A. Artemev, A.G. Khachaturyan, Three-dimensional phase field model of low-symmetry martensitic transformation in polycrystal: simulation of ζ_2'

martensite in AuCd alloys, Acta Mater. 49 (2001) 2309–2320.
[36] L.Q. Chen, Phase-field models for microstructure evolution, Annu. Rev. Mater. Res. 32 (2002) 113–140.
[37] F.E. Hildebrand, C. Miehe, A phase field model for the formation and evolution of martensitic laminate microstructure at finite strains, Philos. Mag. 92 (2012) 4250–4290.
[38] K. Tůma, S. Stupkiewicz, Phase-field study of size-dependent morphology of austenite-twinned martensite interface in CuAlNi, Int. J. Solids Struct. 97–98 (2016) 89–100.
[39] K. Tůma, S. Stupkiewicz, H. Petryk, Size effects in martensitic microstructures: finite-strain phase field model versus sharp-interface approach, J. Mech. Phys. Solids 95 (2016) 284–307.
[40] J.D. Clayton, J. Knap, A phase field model of deformation twinning: nonlinear theory and numerical simulations, Phys. D. 240 (2011) 841–858.
[41] J.D. Clayton, J. Knap, Phase field modeling of twinning in indentation of transparent crystals, Model. Simul. Mater. Sci. Eng. 19 (2011) 085005.
[42] J. Lowengrub, L. Truskinovsky, Quasi-incompressible Cahn-Hilliard fluids and topological transitions, Proc. R. Soc. A 454 (1998) 2617–2654.
[43] A.A. Wheeler, G.B. McFadden, On the notion of a ξ-vector and a stress tensor for a general class of anisotropic diffuse interface models, Proc. R. Soc. A 453 (1997) 1611–1630.
[44] D.M. Anderson, G.B. McFadden, A.A. Wheeler, A phase-field model with convection: sharp-interface asymptotics, Phys. D. 151 (2001) 305–331.
[45] J. Slutsker, K. Thornton, A.L. Roytburd, J.A. Warren, G.B. McFadden, Phase field modeling of solidification under stress, Phys. Rev. B 74 (2006) 014103.
[46] V.I. Levitas, Thermodynamically consistent phase field approach to phase transformations with interface stresses, Acta Mater. 61 (2013) 4305–4319.
[47] V.I. Levitas, K. Samani, Size and mechanics effects in surface-induced melting of nanoparticles, Nat. Commun. 2 (2011) 284.
[48] V.I. Levitas, K. Samani, Coherent solid/liquid interface with stress relaxation in a phase-field approach to the melting/solidification transition, Phys. Rev. B 84 (2011) 140103.
[49] V.I. Levitas, Interface stress for nonequilibrium microstructures in the phase field approach: exact analytical results, Phys. Rev. B 87 (2013) 054112.
[50] V.I. Levitas, Phase field approach to martensitic phase transformations with large strains and interface stresses, J. Mech. Phys. Solids 70 (2014) 154–189.
[51] V.I. Levitas, J.A. Warren, Phase field approach with anisotropic interface energy and interface stresses: large strain formulation, J. Mech. Phys. Solids 91 (2016) 94–125.
[52] K. Momeni, V.I. Levitas, Phase-field approach to nonequilibrium phase transformations in elastic solids via intermediate phase (melt) allowing for interface stresses, Phys. Chem. Chem. Phys. 18 (2016) 12183–12203.
[53] K. Momeni, V.I. Levitas, A phase-field approach to solid-solid phase transformations via intermediate interfacial phases under stress tensor, Int. J. Solids Struct. 71 (2015) 39–56.
[54] E. Fried, G. Grach, An order-parameter-based theory as a regularization of a sharp-interface theory for solid-solid phase transitions, Arch. Ration. Mech. Anal. 138 (1997) 355–404.
[55] D. Schneider, O. Tschukin, A. Choudhury, M. Selzer, T. Böhlke, B. Nestler, Phase-field elasticity model based on mechanical jump conditions, Comput. Mech. 55 (2015) 887–901.
[56] D. Schneider, F. Schwab, E. Schoof, A. Reiter, C. Herrmann, M. Selzer, T. Böhlke, B. Nestler, On the stress calculation within phase-field approaches: a model for finite deformations, Comput. Mech. doi: 10.1007/s00466-017-1401-8.
[57] J.M. Ball, R.D. James, Fine phase mixtures as minimizers of energy, Arch. Ration. Mech. Anal. 100 (1987) 13–52.
[58] K. Bhattacharya, Microstructure of Martensite: Why it Forms and How it Gives Rise to the Shape-memory Effect, Oxford University Press, Oxford, 2004.
[59] A.L. Roytburd, Theory of formation of a heterophase structure under phase transformation in solid state, Sov. Phys. Uspekhi 17 (1974) 326–344.
[60] A.L. Roytburd, J. Slutsker, Deformation of adaptive materials. Part III: deformation of crystals with polytwin product phases, J. Mech. Phys. Solids 49 (2001) 1795–1822.
[61] S. Stupkiewicz, G. Maciejewski, H. Petryk, Low-energy morphology of the interface layer between austenite and twinned martensite, Acta Mater. 55 (2007) 6292–6306.
[62] V.I. Levitas, I.B. Ozsoy, Micromechanical modeling of stress-induced phase transformations. Part 1. Thermodynamics and kinetics of coupled interface propagation and reorientation, Int. J. Plast. 25 (2009) 239–280.
[63] V.I. Levitas, I.B. Ozsoy, Micromechanical modeling of stress-induced phase transformations. Part 2. Computational algorithms and examples, Int. J. Plast. 25 (2009) 546–583.
[64] V.I. Levitas, D.L. Preston, Three-dimensional Landau theory for multivariant stress-induced martensitic phase transformations. I. Austenite ↔ Martensite, Phys. Rev. B 66 (2002) 134206.
[65] V.I. Levitas, D.L. Preston, Three-dimensional Landau theory for multivariant stress-induced martensitic phase transformations. II. Multivariant phase transformations and stress space analysis, Phys. Rev. B 66 (2002) 134207.
[66] V.I. Levitas, D.L. Preston, D.W. Lee, Three-dimensional Landau theory for multivariant stress-induced martensitic phase transformations. III. Alternative potentials, critical nuclei, kink solutions, and dislocation theory, Phys. Rev. B 68 (2003) 134201.
[67] V.I. Levitas, Phase-field theory for martensitic phase transformations at large strains, Int. J. Plast. 49 (2013) 85–118.
[68] V.V. Bulatov, O. Richmond, M.V. Glazov, An atomistic dislocation mechanism of pressure-dependent plastic flow in aluminum, Acta Mater. 47 (1999) 3507–3514.
[69] J.D. Clayton, Nonlinear Mechanics of Crystals, Springer, New York, 2011.
[70] P. Boullay, D. Schryvers, R.V. Kohn, Bending martensite needles in $Ni_{65}Al_{35}$ investigated by two-dimensional elasticity and high-resolution transmission electron microscopy, Phys. Rev. B 64 (2001) 144105.
[71] V.I. Levitas, D.L. Preston, Thermomechanical lattice instability and phase field theory of martensitic phase transformations, twinning and dislocations at large strains, Phys. Lett. A 343 (2005) 32–39.
[72] C.S. Jog, Foundations and Applications of Mechanics, in: Continuum Mechanics, vol. I, Narosa, New Delhi, 2007.
[73] P.C. Clapp, C.S. Becquart, Y. Shao, Y. Zhao, J. Rifkin, Transformation toughening explored via molecular dynamics and Monte Carlo simulations, Model. Simul. Mater. Sci. Eng. 2 (1994) 551–558.
[74] W.S. Slaughter, The Linearized Theory of Elasticity, Springer, New York, 2002.
[75] L. Truskinovsky, Kinks versus shocks, in: J.E. Dunn, R. Fosdick, M. Slemrod (Eds.), Shock Induced Transitions and Phase Structures in General Media, Springer-Verlag, New York, 1993, pp. 185–229.
[76] A. Basak, V.I. Levitas, Supplementary Material for "Interfacial Stresses within Boundary between Martensitic Variants: Analytical and Numerical Finite Strain Solutions for Three Phase Field Models".
[77] I. Steinbach, Phase-field models in materials science, Model. Simul. Mater. Sci. Eng. 17 (2009) 073001.
[78] W. Bangerth, D. Davydov, T. Heister, L. Heltai, G. Kanschat, M. Kronbichler, M. Maier, B. Turcksin, D. Wells, The deal.II library, version 8.4, J. Numer. Math. 24 (2016).